Memoirs of the Faculty of Science, Kyoto University, Series of Physics, Astrophysics, Geophysics and Chemistry, Vol. XXXIII, No. 3. Article 2, 1971.

A COINCIDENCE MEASUREMENT OF NEUTRAL PION ELECTROPRODUCTION THROUGH N^* (1236)

BY

Kota BABA

Department of Physics, Faculty of Science, Hiroshima University

(Received September 10, 1970)

ABSTRACT

Differential cross-sections for the reaction $e+p\longrightarrow e+N^*$ (1236)$\longrightarrow e+p+\pi^\circ$ were measured at the forward angle of the decay proton with respect to the virtual photon direction.

Extracted electrons from the INS 1.3 GeV electron synchrotron were scattered with a liquid hydrogen target and detected by a spectrometer which consists of a sector-type magnet and a counter telescope including a lead glass Čerenkov counter. The decay proton passing through a bending magnet was detected by a time-of-flight system in coincidence with the scattered electrons.

The excitation curves were observed over the N^* (1236) resonance region at the four momentum transfer squared q^2 of $3\mathrm{F}^{-2}$ and for the virtual photon's polarization parameter ε of 0.7 and 0.5. The shape of the excitation curves well coincided with the Dalitz and Yennie's curves.

Using the Rosenbluth plot for the forward cross-section, the contribution of the longitudinal component of the virtual photons seems to be negligiblly small as compared to that of the transverse component.

I. Introduction

In the past more than ten years many experiments of the inelastic electron-proton scattering or electroproduction of pions have been made mainly for the purpose of investigating the electromagnetic structures of pions and nucleon isobars. In the pion-electroproduction process (Fig. 1) an incident electron is scattered by the electromagnetic field of a proton through the exchange of a virtual photon, while the target proton receiving an energy-momentum transfer q by absorbing a photon turns into the final π-N system of invariant mass M. The photoproduction is one of the extreme case where the absorbed photon is real ($q^2=0$), and the elastic electron-proton scattering is another extreme case

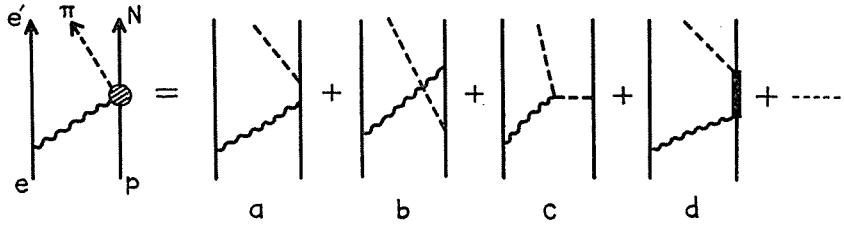

Fig. 1. Feynman diagram of the pion electroproduction from protons.

where the final hadron system is only a proton ($M=938$ MeV). Therefore the electroproduction can be regarded as the extention of the photoproduction and the elastic e-p scattering in the sense that both the two quantities q^2 and M are variable.

The elastic e-p scattering, in which the four-momentum transfer squared, q^2, is non-zero but the energy transfer is zero (in the e-p center-of-momentum system), has been applied to studies of the electromagnetic structure of nucleon in its ground state. The knowledge thus obtained is represented in terms of two form factors G_M and G_E which depend only on q^2. The one photon exchange approximation is well confirmed thus far by the elastic e-p scattering experiments, so that the same approximation is assumed also for the electroproduction.

The electroproduction contains more various informations on electromagnetic properties of hadrons. The spatial structure of nucleon isobars can be probed by the reaction $e+p\longrightarrow e+N^*$ ($N^*\longrightarrow N+\pi$), in which the target proton is excited into a resonance state by absorbing a virtual photon (Fig. 1 d). The virtual photon, in addtion to its non-vanishing mass, has a longitudinal (or scalar) component and is polarized transversely and longitudinally, so that the excitation mechanism of nucleon isobars can be investigated from a more general point of view than with real photons. The electroproduction process in which a virtual photon is absorbed by a peripheral pion (Fig. 1 c), on the other hand, is related to the pion form factor, hence providing an important tool for investigating the electromagnetic structure of the pion. The pion, being a spin-zero particle, has one form factor, while the nucleon isobar N^* (1236), of which the spin is assigned as 3/2, has three form factors.

Form an experimental view point there are two types of the electroproduction experiments, those performed by detecting the scattered electrons only and those performed by detecting a final hadron in coincidence with the scattered electron. The former is essentially a simple missing-mass spectroscopy and does not distinguish the final hadron states of $p+\pi^\circ$, $n+\pi^+$, etc. The quantity observed gives the total cross-section for absorption of the virtual photon. Since the work of Panofsky and Allton[1] the experiments of this type have been performed in many laboratories[2),3)], in which the nucleon resonance peaks have been observed up to the third resonance and the relating multipoles have been discussed to some extent in connection with the threshold relations. But more precise treatments of resonance excitations, such as the separation of the three form factors of N^* (1236), or the determination of the pion form factor, can not be made by detecting the scattered electrons only but require the coincidence experiments in which generally the angular distribution of the virtual-photoproduction is to be observed.

The experimental works intending to determine the form factors of pion and nucleon isobars have been reported by a few groups[4)~6)] recently, although the coincidence experiments are much more complicated than the single arm experiments.

We report here a preliminary experiment*) on the reaction

$$\begin{aligned} e+p&\longrightarrow e+N^*\ (1236)\\ &\quad\ \big\lfloor\!\longrightarrow p+\pi^\circ, \end{aligned} \tag{1}$$

*) This experiment was reported briefly in ref. (7).

which was performed by deteting the forwand proton (with respect to the virtual photon direction) and the scattered electron in coincidence. In the forward direction one of the transverse form factors, f_+, does not contribute as described later, and consequently the scalar component is relatively enhanced. Taking advantage of this situation the aim of this experiment was to determine separately the rest two of the three form factors, f_- and f_c, of the γpN^* (1236) vertex simply by observing the forward crossections.

II. Theoretical Background

1. Kinematics

The Feynman diagram of the reaction (1) is shown in Fig. 2, in which p, p', q, P, P' and p_π denote the energy-momentum four vectors of each particles. The kinematical variables determined directly by detecting the scattered electrons are the initial and the final energies, p_0 and p_0' (we write these as $p_0=\omega$, $p_0'=\omega'$), and the scattering angle θ of electrons in the laboratory frame. From these three electron variables ω, ω' and θ, with the constant quantity of

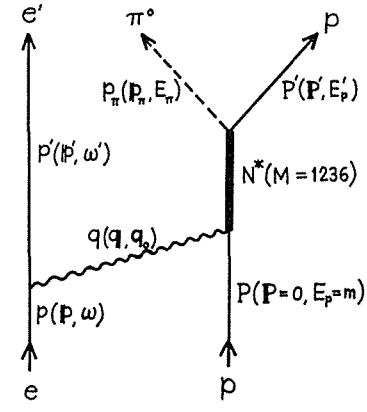

Fig. 2. Feynman diagram of the neutral pion electroproduction via N^* (1236).

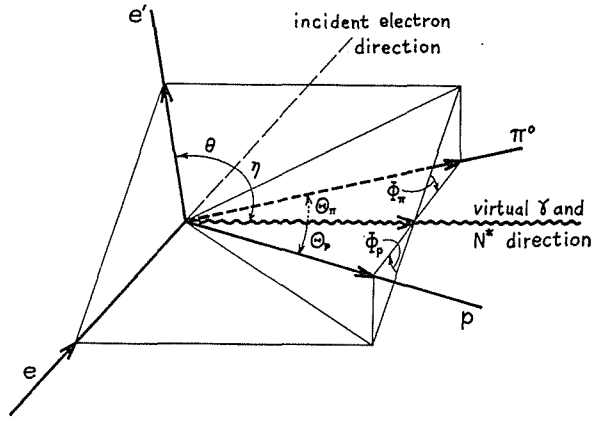

Fig. 3. Illustration of the angle of each particle in the laboratory frame.

target mass m, one can determine another set of three independent quantities q^2, ε and M convenient for theoretical treatments.

Firstly an invariant quantity q^2, the four-momentum transfer squared, is defined by

$$q^2=(p-p')^2=\boldsymbol{q}^2-q_0^2=\boldsymbol{q}^{*2}-q_0^{*2},$$

where $\boldsymbol{q}$ and q_0 are the three-momentum and the energy of the virtual photon in the laboratory system (ls), and $\boldsymbol{q}^*$ and q_0^* are those in the center-of-momentum system (cms) of the virtual photon and the proton. Using the above metric for q, q^2 is positive in the space like region (as in the electroproduction). In the approximation of electron mass $m_e=0$, q^2 is expressed in terms of ω, ω' and θ as follows:

$$q^2=2\,\omega\omega'(1-\cos\theta). \tag{2}$$

Secondly a parameter ε, which represents the degree of transverse polarization of the virtual photon, is defined as

$$\varepsilon=\frac{|j_x|^2-|j_y|^2}{|j_x|^2+|j_y|^2},$$

where j_x is the component of the electron current perpendicular to the virtual photon direction in the electron's scattering plane and j_y is the component perpendicular to both the virtual photon direction and the scattering plane. The transverse polarization ε is invariant under Lorentz transformation along the virtual photon direction (z-direction), while the longitudinal polarization varies by Lorentz transformation along z-direction and is defined, for example, as $q^2/q_0^2\cdot\varepsilon$ in the laboratory frame. The factor q^2/q_0^2 comes from the continuity condition which combines the longitudinal component and scalar component. The expression of ε is given by

$$\varepsilon=\left[1+2\frac{|\boldsymbol{q}|^2}{q^2}\tan\frac{2\theta}{2}\right]^{-1}, \tag{3}$$

where $\boldsymbol{q}$ is written as

$$|\boldsymbol{q}|^2=|\boldsymbol{p}-\boldsymbol{p}'|^2=\omega^2+\omega'^2-2\,\omega\omega'\cos\theta.$$

These two quantities q^2 and ε represent the characters of the virtual photon and are given by the same expressions as those for the elastic e-p scattering since they depend only on the electron variables.

Another invariant quantity M is the mass of N^*, or in other words, the total energy of the virtual photon-proton or the final pion-nucleon system in the cms. This is defined by

$$M^2=(q+P)^2=(p_\pi+P')^2,$$

and can be written as

$$M^2=m^2+2mq_0-q^2, \tag{4}$$

where $q_0=\omega-\omega'$, and m is the mass of proton.

It should be noted that the above three quantities q^2, ε and M are independent to each other so that one can determine first the values of q^2, ε and M freely, for which the corresponding set of electron variables ω, ω' and θ

are found by the following equations:

$$\omega=\frac{1}{2}\left(\sqrt{\frac{1+\varepsilon}{1-\varepsilon}}|\boldsymbol{q}|+q_0\right), \tag{5}$$

$$\omega'=\frac{1}{2}\left(\sqrt{\frac{1+\varepsilon}{1-\varepsilon}}|\boldsymbol{q}|-q_0\right), \tag{6}$$

$$\cos\theta=\frac{\varepsilon(2q_0{}^2+3q^2)-q^2}{\varepsilon(2q_0{}^2+q^2)+q^2}, \tag{7}$$

where q_0 is to be written as $q_0=(M^2-m^2+q^2)/2m$.

The direction of the three-momentum transfer vector $\boldsymbol{q}$, along which the

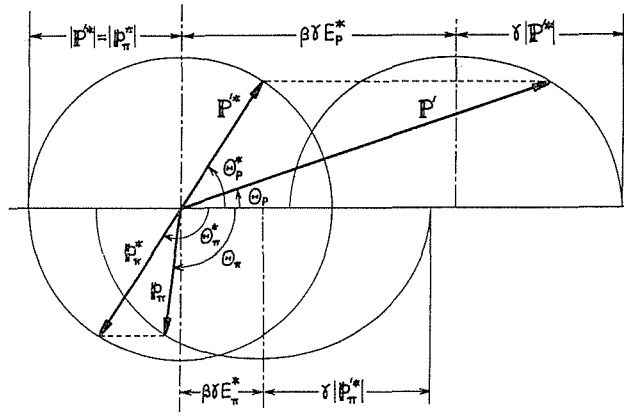

Fig. 4. Graphical illustration showing the relations between the momentum and the angle in the cms and those in the ls. The length of arrow corresponds to the amount of the momentum.

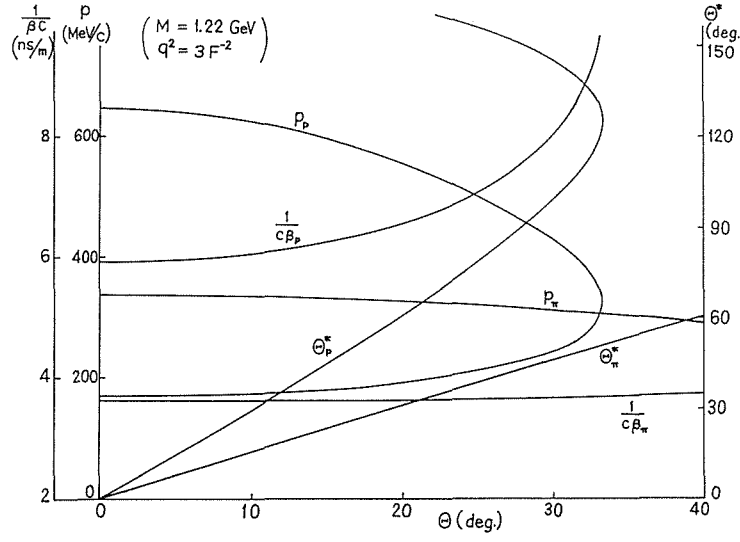

Fig. 5. Momentum, velocity and θ^* of protons and pions vs θ. An example for $q^2=3\text{F}^{-2}$ and $M=1.22$ GeV is shown. The lower value of proton momentum corresponds to the proton emitted backward in the cms.

virtual photon is emitted, has an angle η given below with respect to the incident electron beam:

$$\sin\eta=\frac{\omega'}{|\boldsymbol{q}|}\sin\theta=\frac{\sqrt{q^2}}{2\omega}\sqrt{\frac{2\varepsilon}{1-\varepsilon}}. \tag{8}$$

As the direction of the virtual photon corresponds to that of the incident beam in the real photoproduction, it is natural that the emitting angles of the final pion and nucleon are defined with respect to this axis as shown in Fig. 3. We denote the polar and the azimuthal angles of the final proton in the ls by θ_p and Φ_p' and those in the cms of the final π-N system by θ_p^* and $\Phi_p^*(=\Phi_p)$. Since the number of the independent kinematical variables contained in the reaction $e+p\longrightarrow e+N+\pi$ is five disregarding the spin, one can define the reaction completely by the above mentioned five variables ω, ω', θ, θ_p^* and Φ_p^*.

Some other useful kinematical relations are listed below and illustrated in Fig. 4 and Fig. 5.

Virtual photon momentum (cms);

$$|\boldsymbol{q}^*|^2=\frac{m^2}{M^2}|\boldsymbol{q}|^2=q^2+\frac{1}{4M^2}(M^2-m^2-q^2)^2$$

Final proton or pion momentum (cms);

$$|\boldsymbol{P}'^*|^2=|\boldsymbol{p}_\pi|^2=\frac{1}{4M^2}\Big[M^2-(m+\mu)^2\Big]\Big[M^2-(m-\mu)^2\Big]$$

μ; pion mass

Energy of N^* (ls);

$$\boldsymbol{E}^2=M^2+|\boldsymbol{q}|^2=(m+q_0)^2$$

Velocity of the cms or N^* (ls);

$$\beta=\frac{|\boldsymbol{q}|}{\boldsymbol{E}}=\frac{|\boldsymbol{q}|}{m+q_0}$$

Lorentz factor of the cms or N^* (ls);

$$\gamma=\frac{E}{M}=\frac{m+q_0}{M}$$

Final proton momentum (ls);

$$|\boldsymbol{P}'|=\sqrt{|\boldsymbol{P}'^*|^2\sin^2\Theta^*+\gamma^2(|\boldsymbol{P}'^*|\cos\Theta^*+\beta E_p^*)^2}$$

E_p^*; proton energy in the cms

Final proton angle (ls);

$$\Theta_p=\tan^{-1}\left[\frac{|\boldsymbol{P}'^*|\sin\Theta_p^*}{|\boldsymbol{P}'^*|\cos\Theta_p^*+\beta E_p^*}\right]$$

Jacobian factor;

$$\begin{aligned}\frac{d\Omega^*}{d\Omega}&=\frac{\pm[\sin^2\Theta^*+\gamma^2(n+\cos\Theta^*)^2]^{3/2}}{\gamma(1+n\cos\Theta^*)}\\&=\frac{\pm(1-\beta^2)[n\cos\Theta\pm\sqrt{1-\gamma^2(n^2-\beta^2)\sin^2\Theta}]^2}{(1-\beta^2\cos^2\Theta)^2\sqrt{1-\gamma^2(n^2-\beta^2)\sin^2\Theta}}\\&=\gamma^2(1+n)^2\quad\text{at }\theta=0\end{aligned}$$

$$n=\begin{cases}\dfrac{\beta\sqrt{|\boldsymbol{P}'^*|^2+m_2}}{|\boldsymbol{P}'^*|} & \text{for proton}\\[2ex] \dfrac{\beta\sqrt{|\boldsymbol{P}'^*|^2+\mu_2}}{|\boldsymbol{P}'^*|} & \text{for pion}\end{cases}$$

2. Cross Section Formula

There are a number of the cross-section formulas for the inelastic electron scattering calculated by many authors with the assumption of one photon exchange. Hand's formula[2] is one of those which are often cited in references:

$$\begin{aligned}\frac{d\sigma}{d\Omega d\omega'}&=\Gamma_t(q^2,\ K)\sigma_t(q^2,\ K)+\Gamma_0(q^2,\ K)\sigma_0(q^2,\ K)\\&=\frac{\alpha^2}{4\pi}\frac{K}{q^2}\frac{\omega'}{\omega}\frac{1-\varepsilon}{2}[\sigma_t+\varepsilon\sigma_0]\end{aligned}\tag{9}$$

where α is the fine structure constant 1/137, and K $(=q_0-q^2/2m)$ is the energy of the real photon equivalent (giving rise to the same M) to the virtual photon of energy q_0. This formula gives the cross-section for the detection of scattered electrons only, where the kinematical factors Γ_t and Γ_0 come from the electron-photon vertex while σ_t and σ_0 come from the photon-hadron vertex corresponding to the absorption of purely transverse and purely longitudinal (or scalar) photons, respectively. Since Γ_t and Γ_0 can be interpreted as the numbers of transverse and longitudinal photons per MeV·steradian, respectively, the polarization parameter $\varepsilon(=\Gamma_0/\Gamma_t)$ is also considered as the relative intensity of longitudinal photons to transverse photons.

We have another formula given by Bjorken and Walecka[8]:

$$\frac{d\sigma}{d\Omega}=\frac{\alpha^2}{q_2}\frac{\omega'}{\omega}\frac{\omega'}{\omega-\dfrac{M^2-m^2}{2m}}\frac{M^2}{m^2}\frac{2}{1-\varepsilon}\left\{\frac{1}{2}\left[f_+^2(q^2)+f_-^2(q^2)\right]+\frac{\varepsilon q^2}{|\boldsymbol{q}^*|^2}f_0^2(q^2)\right\},\tag{10}$$

which gives the cross-section for the electroproduction of N^* by detecting the scattered electrons only. In this formula Bjorken and Walecka defined the form factors f_+, f_- and f_c corresponding to the transition from the nucleon of helicity 1/2 to the isobar of helicity 3/2, $-1/2$ and 1/2, respectively. Since the final state is considered as the nucleon isobar of a definite mass M, the cross-section formula is written in the form analogous to the well-known Rosenbluth formula for the elastic scattering as written in terms of the polarization parameter ε:

$$\frac{d\sigma}{d\Omega}=\frac{\alpha^2}{q^2}\left(\frac{\omega'}{\omega}\right)^2\frac{2}{1-\varepsilon}\left[\frac{q^2}{4m^2}G_M^2+\varepsilon\cdot G_E^2\right].\tag{11}$$

These cross-section formulas (9)~(11) have essentially the same form about ε, and the transverse-longitudinal or tranverse-scalar separation is attained by the recipe of so-called Rosenbluth plot.

For coincidence experiments the cross-section is triply differentiated and the separation into purely transverse and purely longitudinal parts does not hold. This is due to the appearance of the interference terms, which disappear in the detection of scattered electrons alone on account of the integration over the azimuthal angle. Christ and Lee[9] showed a theorem in the Appendix A of ref. (9) which describes the cross-section for the process where an N^* of

arbitrary spin is electroproduced and decays into a nucleon and a pion. Following their theorem the differential cross-section for reaction (1) can be written in terms of the form factors $f_{\pm}$ and f_c [10]:

$$d\sigma=\frac{\alpha^2}{12\pi}\frac{1}{q^2}\frac{\omega'}{\omega}\frac{M^2}{mE}\frac{1}{1-\varepsilon}d\omega' d\Omega_e\delta(E+\omega'-\omega-m)d\Phi^* d\cos\theta^*.$$
$$\Big[3f_+^2\sin^2\theta^*+f_-^2(1+3\cos^2\theta^*)+2\frac{q^2}{|\boldsymbol{q}^*|^2}\varepsilon f_c^2(1+3\cos^2\theta^*)$$
$$+2\sqrt{3\varepsilon}R_e(f_+f_-^*)\sin^2\theta^*\cos 2\Phi^*-4\sqrt{3}\sqrt{\frac{q^2}{|\boldsymbol{q}^*|^2}}\sqrt{\varepsilon(1+\varepsilon)}R_e(f_+f_c^*).$$
$$\sin\theta^*\cos\theta^*\cos\Phi^*\Big]. \tag{12}$$

The first two terms in the bracket are due to unpolarized purely transverse photons and the third term is due to purely scalar (or longitudinal) photons. The next term proportional to $\cos 2\Phi^*$ represents the effect of transverse-transverse interference and can be also observed in the photoproduction by polarized real photons. The last term in the bracket represents the contribution of transverse-scalar interference and is observed only in the coincidence measurement of the electroproduction.

In order to determine the three form factors $f_{\pm}$ and f_c separately, it is necessary to observe the angular distributions with respect to both the polar and the azimuthal angles. It is seen from eq. (12), however, that one of the transverse form factors, f_+, does not contribute at $\theta^*=0$, and hence the interference terms also vanish there. Therefore the cross-section for the process in which the decay proton is emitted at the forward angle is reduced to be:

$$\frac{d^3\sigma(\theta^*=0)}{d\omega' d\Omega_e d\Omega^*}=\frac{\alpha^2}{3\pi}\frac{1}{q_2}\frac{\omega'}{\omega}\frac{M^2}{mE}\frac{1}{1-\varepsilon}\delta(E+\omega'-\omega-m)\Big[f_-^2+2\frac{q^2}{|\boldsymbol{q}^*|^2}\varepsilon f_c^2\Big], \tag{13}$$

where Ω_e and Ω^* are the solid angle for the scattered electron in the ls and that for the decay protons in the cms, respectively. This formula again has a common form with the cross-section formulas (9)~(11). The form factors f_- and f_c can be separated by the Rosenbluth plot without observing the whole angular distribution.

Since N^* is considered as a real particle with the definite mass M in the above formula, E has a definite value corresponding to M when q^2 is fixed, and consequently the above expression gives a δ-function-like cross-section, although the actual cross-section is given by a resonance curve with a finite width. Then it will be reasonable to assume that the integral of the δ-function can be substituted by that of the actual resonance curve, and we have[11]

$$f^2(q^2,\varepsilon)\equiv f_-^2(q^2)+2\frac{q^2}{|\boldsymbol{q}^*|^2}\varepsilon f_c^2(q^2)$$
$$=\frac{3\pi}{\alpha^2}q^2\frac{\omega}{\omega'}\frac{m^2}{M^2}(1-\varepsilon)\int_{\substack{\text{over resonance}\\ q^2,\ \varepsilon=\text{fixed}}}\frac{d^3(\theta^*=0)}{d\omega' d\Omega_e d\Omega^*}dE \tag{14}$$

Here the integration of the cross-section over E should be made at a fixed q^2 and ε. In the experiment the forward cross-section $d^3\sigma(\theta^*=0)/d\omega' d\Omega_e d\Omega^*$ should be measured for various values of E (hence, for M) over the resonance curve but keeping q^2 and ε cnstant. This implies that ω, ω' and θ must be varied

for each data point. For the remaining factors ω, ω', M and q^* in eq. (14), however, the values corresponding to the resonance peak $M=1236$ MeV (and of course to given q^2 and ε) are to be substituted. This would be justified simply because we have assumed that the form factors are functions of q^2 only and not of the isobar mass. Thus, in principle, by obtaining $f^2(q^2, \varepsilon)$ for at least two values of ε the form factors $f_-^2(q^2)$ and $f_c^2(q^2)$ can be determined separately.

III. Experimental Apparatus and Procedure

1. Beam

The experiment was carried out with the external beam of the 1.3 GeV electron synchrotron of Institute for Nuclear Study (INS), University of Tokyo. The beam was extracted from the synchrotron ring by the resonance method and transported through a system consisting of bending magnets, slits and quadrupole magnets. A detailed description of the beam extraction and transport system has been given by K. Huke et al.[12]

The incident beam energy was defined by a pair of analyzing magnets and a slit of the beam transport system. The energy spread including the time variation was estimated to be at most $\pm 1.2\%$. The beam profile at the target position did not exceed a circle of 10 mm in diameter. The fluctuation of the beam position was at most ± 4 mm.

The duty time of the extracted beam was about 1 ms in each repetition cycle of 21.3 cps. The beam often showed the time structure having some sharp spikes in a burst, which caused higher accidental coincidence rates. We were even obliged to reduce the beam intensity by a factor of ten, in the worst case, to avoid lower data quality.

The beam intensity was measured by using a secondary emission monitor (SEM) located in front of the liquid-hydrogen target chamber. The SEM consisted of seven layers of 10 μm thick aluminum foils and was held in the vacuum of $3\sim5\times10^{-4}$ mmHg. The efficiency of the SEM was calibrated with a quantameter within an error of $\pm 1\%$. The average beam intensity during the course of the experiment was about 10^{11} electrons per second.

2. Target

The liquid-hydrogen target was that of Whalin and Reitz type[13]. The appendix was a horizontal cylinder made of 250 μm thick mylar film, and its dimension was 11 cm in length and 6 cm in diameter. The entrance window of the target chamber was made of two folded mylar films separated by 1.5 cm from each other. In order to prevent possible accidents caused by radiation damages, the outer window was renewed every week. For the exit window stainless steel foil of 50 μm thick was used for the sake of safety.

3. Electron Spectrometer

Figure 6 shows the experimental set-up schematically. The scattered electrons were momentum-analyzed with a magnet of sector type. The central orbit of the electrons was normal to the entrance and exit edges of the magnetic field, and was deflected by 50 degrees. The electrons after passing through the magnet were detected by four-fold coincidence (referred to as the e-coincidence) of scintillation counters EH 1, ES 1, ES 2 and a leadglass Čerenkov counter.

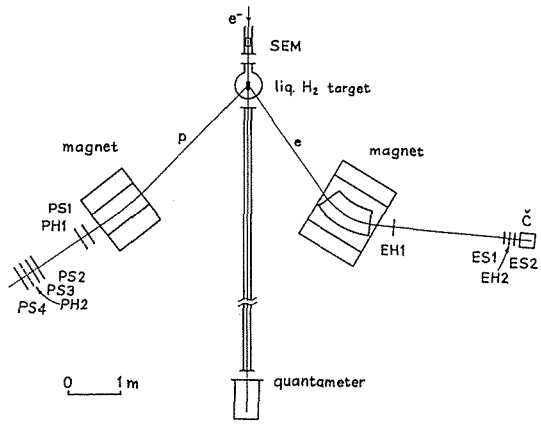

Fig. 6. The experimental arrangement. S: scintillation counter; H: hodoscope; Č: lead-glass total absorption Čerenkov counter.

Counter EH 1 consisted of three vertical slats of 5 mm thick plastic scintillator viewed by phototubes of 6655A. This counter was placed right behind the magnetic field and defined the horizontal angular width, while the vertical angular width was defined by the exit pole edges of the magnet. Counters ES 1 and ES 2 were made of a 10 mm thick plastic scintillator and viewed by a phototube of 56 AVP. Counter ES 1 was placed at the focal plane and used to define the total momentum acceptance. The characters of the magnetic focusing system, such as the focal length, the momentum dispersion, etc., were measured by the floating-wire method, from which the momentum acceptance $\Delta p/p$ and the solid angle $\Delta\Omega_e$ were found to be 9.2 % and 3.6×10^{-3} sr, respectively, for the point source. The phase space diagram limited by these counters is shown in Fig. 7.

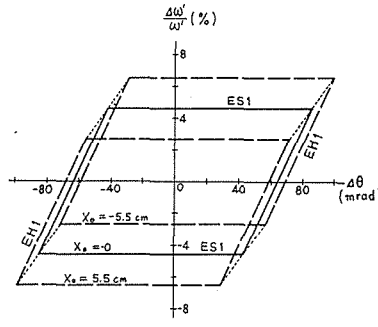

Fig. 7. The phase space for the electron telescope. The region defined by counters ES1 and EH1 is detected. X_0: displacement at the target perpendicular to the central orbit of scattered electrons.

The lead-glass Čerenkov counter was used to identify electrons. It had the size of 30 cm in length and 40 cm in diameter and was viewed by four phototubes of 58 AVP which were adjusted to give the same gain. The discrimination level for the Čerenkov pulse was made sufficiently low so as to avoid counting loss at the lower tail of the electron peak. The decrease of

the pulse height at the off-axis incidence to the Čerenkov counter was found to be sufficiently small[14]. Thus the counting efficiency for electrons of the Čerenkov counter can be considered to be 100 %.

Counter EH 2 consisted of five vertical slats of 10 mm thick plastic scintillator viewed by phototubes of 6199. This counter as well as EH 1 served as hodoscopes to give informations about the particle trajectory.

4. Proton Telescope

In the proton telescope, positively charged particles which were bent 11.5° by a rectangular magnet were detected by four-fold coincidence (referred to as the p-coincidence) of scintillation counters PS 1~PS 4. As the opening angle of the proton telescope was sufficiently small, the protons detected by the proton telescope in coincidence with the scattered electrons had nearly constant momentum disregarding the protons emitted backward in the cms (see Fig. 5). Therefore the magnet was used mainly to eliminate the background particles, especially the electrons scattered elastically.

Counters PS 1 and PS 2~4 were composed of plastic scintillator of 5 mm and 10 mm in thickness, respectively, and viewed by phototubes of 56 AVP. Hodoscopes PH 1 and PH 2 were divided into four vertical counters of 5 mm thick plastic scintillators viewed by phototubes of 6655 A. The phase space of the proton arm was limited by counters PS 1, PS 4 and the aperture of the magnet as shown in Fig. 8. The solid angle was estimated to be 2.7×10^{-3} sr for the point source, by the floating-wire method.

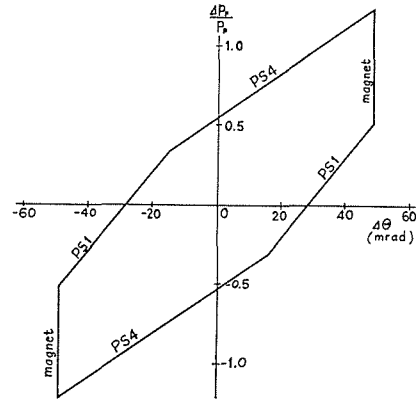

Fig. 8. The phase space for the proton telescope. The detected region is defined by counters PS 1, PS 4 and the magnet aperture.

The signals of the e- and p-coincidence were again counted in coincidence (referred to as the ep-coincidence). The resolving time of the ep-coincidence was made fairly large (about 55 ns) so that the positive pions from the reaction $e+p\rightarrow e+n+\pi^+$ can be also counted as well as for protons.

To distinguish protons from positive pions, the time differences between the signals of ES 1 and PS 4 were measured with a time-to-pulse-height converter gated by the ep-coincidence. The linearity and the time scale of the time-to-pulse-height converter were checked frequently and found to be constant during our experiment.

Although no definite measurements were made on the counting efficiency of the proton telescope, it was assumed to be 100 per cent, because the discrimination level was set low enough so that the proton peak is fully observed in the pulse height spectrum.

5. Electronic Circuits and Computer System

A simplified block diagram of the fast electronic circuits and computer system is shown in Fig. 9. Most of the fast circuits used were the standard circuits of INS high energy division*), of which the rise time was usually about 3 ns. The signals of each counter were clipped by a 5 ns cable at the terminal of the counter box.

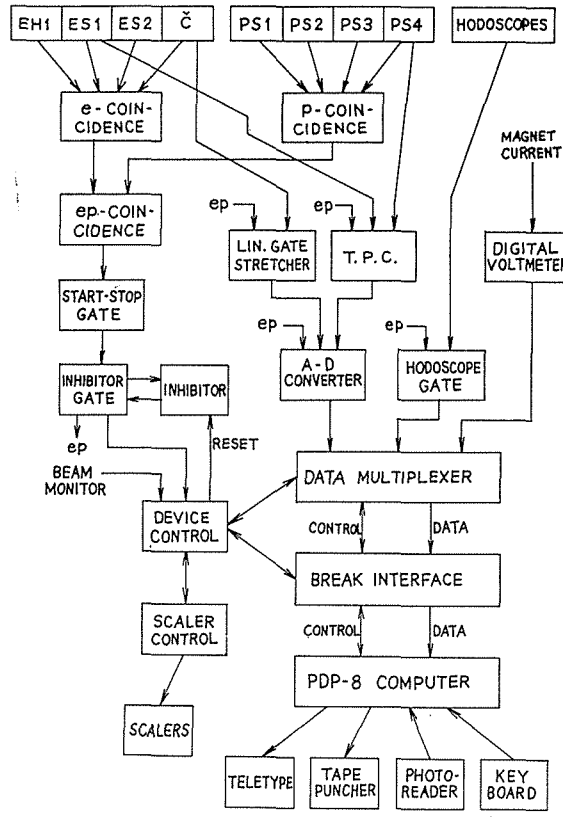

Fig. 9. A simplified block diagram of the fast electronics and the data recording system.

Data taking was done as follows using a DEC PDP-8 computer. Each time the *ep*-coincidence was counted, the following informations were punched out on the paper tape through an on-line system of PDP-computer.

i) The pulse height of the lead-glass Čerenkov counter.

ii) The pulse height of the time-to-pulse-height converter. (These two

*) The time-to-pulse-height converter was lent through the courtesy of Kyoto University High Energy Physics Laboratory.

were converted to channel numbers through ND-160 F 64 channel AD-converters.)

iii) The responses of the four hodoscopes.

iv) The excitation current of the analyzing magnet in the electron telescope.

v) Other necessary informations such as the run number, etc.

The data multiplexer can store large bits of data (up to 288 bits) which arrive in simultaneously from AD-converters and hodoscope gates, etc., and send out by 48 bits under the control of the break interface. The break interface functions as follows: When received the signal of the *ep*-coincidence the break interface brings the computer into the 'data break state', in which the externanl data stored in the interface are transferred not by the soft ware control but by the hard wares directly to the core memory of the computer. The detailed description of the interface and the multiplexer have been given by N. Kajiura[15].

The 'device control' was used in order to concentrate the control of start, stop and reset operations of the multiplexer and the interface as well as the scalers. The time required for the computer system to handle one event was about 70 μs, during which the inhibitor gate was closed. This was negligible as compared to the *ep*-counting rate of one count per three minutes in the case of the maximum rate.

IV. Data Reduction

1. Event Identifications

The informations of the recorded *ep*-events were analyzed in various manner. The events of which the pulse height of the Čerenkov and time-of-flight corresponded to the correct electron and proton peaks, respectively, were identified as true electronproton coincidence events. The consistency of the configurations of responses from the hodoscopes was also taken into account in identifying the events.

Figure 10 a shows an example of the pulse height spectrum of the Čerenkov counter for the *ep*-coincidence events. In order to define the correct position of the electron peak, the Čerenkov spectrum gated by the *e*-coincidence signal only was observed in each condition of the experiment. Figure 10 b shows this spectrum corresponding to Fig. 10 a. The rise of the lower side tail is considered to be due to negative pions which might be produced by real photons in the target. This was confirmed by the Čerenkov spectrum of Fig. 10 c, which were observed by reversing the magnetic field, showing the peak of positive pions produced by real photons.

An example of the time-of-flight spectrum is shown in Fig. 11 a. A direct identification of the proton peak was made at one experimental condition by inserting copper absorbers of thickness just sufficient to stop the protons.

2. Background Subtraction

The dashed line in Fig. 11 a indicates the random background level, which was determined from the counting rate of the accidental *ep*-coincidence. The distribution was estimated from the single rate of the 'stop counter' PS 4. The random background for the TOF spectrum will have uniform distribution

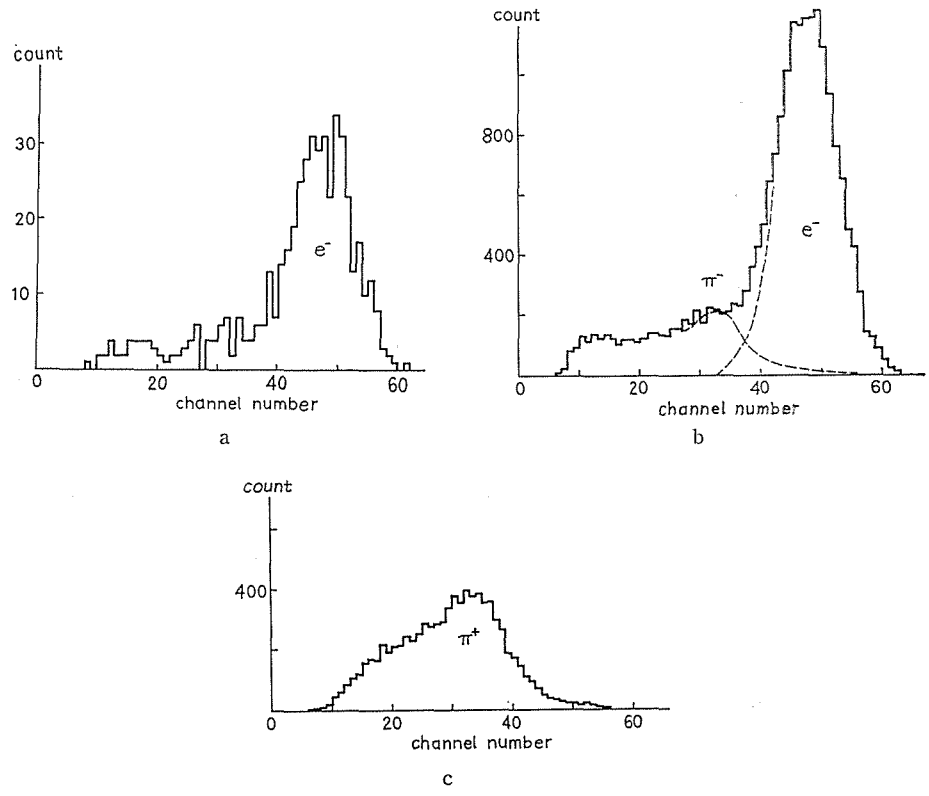

Fig. 10. Examples of the pulse height spectra of the Čerenkov counter.
a Gated by the *e-p* coincidence signal.
b Gated by the *e*-coincidence signal.
c Gated by the *e*-coincidence signal, but the polarity of the analyzing magnet was reveresed.

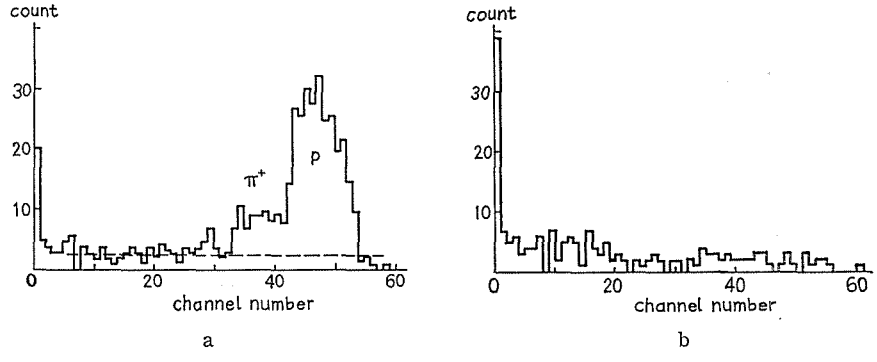

Fig. 11. Examples of the pulse height spectra of the time-to-pulse height converter.
a A spectrum for '*ep*'-events with the Čerenkov pulse height corresponding to the electron peak.
b Gated by the accidental *e-p* coincidence signal under the normal beam condition.

if the average pulse interval of the 'stop counter' is long enough as compared with the duration of the gate pulse. Under the normal beam condition of the present experiment the random background was observed to have nearly uniform distribution as shown in Fig. 11 b.

The *ep*-coincidence rate with an empty target was observed at one experimental condition to be 4.4 ± 1.9 % of that with a full target.

3. Elastic Scattering Measurement

The elastic *e-p* scattering measurement was made by the electron telescope only in order to check the overall operation of the electron detecting system. The momentum spectrum of the elastically scattered electrons was observed at the scattering angle of 48° for the incident energy of 800 MeV by varying the excitation current of the analyzing magnet. The expected spectrum was calculated for the phase space mentioned before, using the well-established cross-section for the *e-p* elastic scattering and the radiative corrections basing on the formulas given by Allton[16]. The effects due to the fluctuation of the magnet current and the multiple scattering of electrons in the beam path were also taken into account. The calaulated spectrum was fairly in good agreement with the observed spectrum as shown in Fig. 12. The counting efficiency of

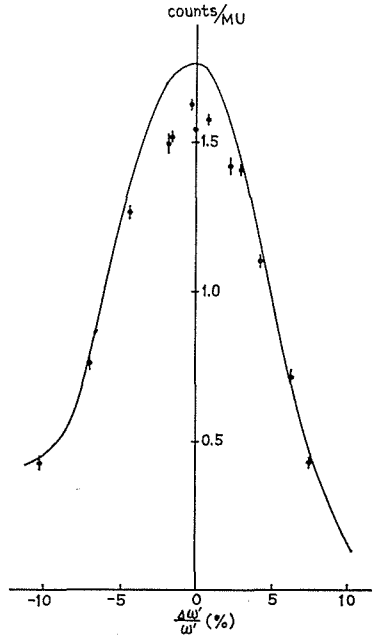

Fig. 12. The momentum spectrum of the elastically scattered electrons observed at the condition of $\omega=800$ MeV, $\theta=48°$. Solid line shows the expected spectrum calculated for the phase space of the electron telescope.

the electron telescope was found to be 92.6 ± 2.8 %. These calculations were done mainly by R. Hamatsu[17].

4. Radiative Correction

Since the experimentally observed high energy electron-proton scattering

events are always accompanied with radiation of one or more photons, the radiative corrections have to be made to obtain the true cross-section. The radiative processes to be considered are divided in two categories; the radiation from the electron by physical radiators such as the target walls before and/or after the scattering and the radiation during the scattering process itself, which are sometimes called the external and the internal bremsstrahlung, respectively. Usually the "peaking approximation" can be made for both the external and the internal bremsstrahlung, which assumes that all the photons emitted are parallel to either incident or scattered electrons, that is, electrons are not altered their direction of motion via radiation but only degraded their energies. Though the internal bremsstrahlung is independent of the thickness of the target material, it can be treated in the same way as the external bremsstrahlung[18] by introducing the equivalent radiator as in the expression (15).

In the inelastic e-p scattering the distortion of the experimental yield from the true cross-section is twofold: by radiating 'out' of and 'in' to the detection system having a momentum width of $\Delta\omega'$. The former is the case that the electrons scattered with the proper M of interest, fail to be detected within a momentum width of $\Delta\omega'$ on account of the energy degradation by radiation. The correction for this is usually written as δ in the factorized form;

$$\sigma_{exp}=\sigma_0(1-\delta).$$

Since the momentum acceptance of the proton telescope was very wide in the present experiment, the momentum resolution of the proton detection system was not taken into account on calculating δ. Therefore it can be assumed that the expression of δ for the elastic scattering cross-section[19] is valid also for the triply differentiated cross-section. Thus the radiative correction for this part is written as

$$\frac{d^3\sigma}{d\omega' d\Omega_e d\Omega^*}\Big)_{exp}=\frac{d^3\sigma}{d\omega' d\Omega_e d\Omega^*}\Big)_{true}\cdot(1-\delta),$$

where

$$\delta=\frac{-2\alpha}{\pi}\left\{\left(\ln\frac{\omega'}{\Delta\omega'}+\frac{1}{2}\ln\frac{\omega'}{\omega}-\frac{13}{12}\right)\left(\ln\frac{q_2}{m_e^2}-1+\frac{t_b+t_a}{\ln_2}\frac{\pi}{\alpha}\right)+\right.$$
$$\left.+\frac{1}{4}\left(\ln\frac{\omega}{\omega'}\right)^2+\frac{17}{36}\right\}. \qquad (15)$$

In this expression the external radiation by physical materials of t_b and t_a (in radiation length) before and after the scattering center, respectively. The internal radiation is treated in the same way by the equivalent radiator of $\ln 2\frac{\alpha}{\pi}\left(\ln\frac{q^2}{m_e^2}-1\right)$. The radiative corrections estimated from eq. (15) amounted to about 15 % for $\varepsilon=0.7$ and about 13 % for $\varepsilon=0.5$.

Figure 13 illustrates the case of "radiating in", in which either the electrons, scattered with lower isobar mass M_1 (therefore having higher energy ω_1'), are degraded their energy by radiation, or radiate first and are scattered with lower isobar mass M_1. In both cases the electrons are detected with the proper final energy ω'. For the present experiment, in which the electrons and protons were detected in coincidence, the effects of this latter case are expected to be very small: In the region of the $M=1236$ resonance, the major part of the "radiating in" from lower isobar mass is associated with $M_1=938$

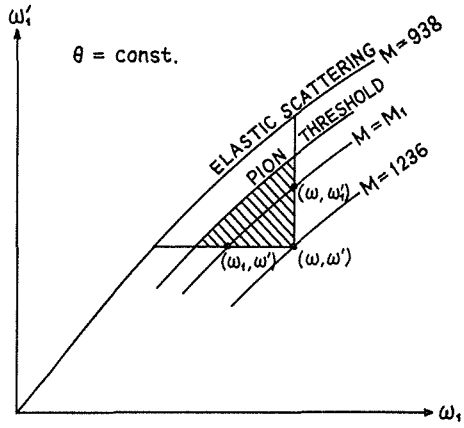

Fig. 13. Kinematically allowed region for scattering in presence of radiation. An electron of initial energy ω is scattered, radiating before and/or after the scattering, with $M=M'$ and is detected with final energy ω'.

MeV and appears as the radiative tail of the elastic scattering. Since the angles of the proton telescope were quite different from those of the recoil protons from the elastic scattering accompanied with radiation, these events were not counted in the present experiment. For the shaded area of Fig. 13 the integration over ω_1 and ω_1' is necessary according to the Bjorken's recipe[18]. But the "radiating in" from this area to the resonance peak is considered to be very small.

5. Nuclear Absorption

Some fractions of protons are absorbed with the materials along the beam path. The probarbility that the protons survive without being absorbed by the materials is given by

$$\eta=\exp(-\sigma_a Nx/A),$$

where N is the Avogadro number, x and A are the thickness in gr/cm^2 and the mass number of the material, respectively, and σ_a is the nuclear absorption cross-section.

Since the large part of the nuclear absorption cross-section is due to small angle scattering, the correction was applied for the materials in the proton path from the target to the counter PH 1, of which the major part consisted of plastic scintillators (polystylene) and air. The cross-section for the nuclear absorption of protons of 100~200 MeV by these materials have a nearly constant value of about 200 millibarn. The nuclear absorption correction was estimated to be 3 %.

6. Cross-section

The triply differentiated cross-section is given by

$$\frac{d^3\sigma}{d\omega' d\Omega_e d\Omega^*}=\frac{Y\eta_e\eta_p(1-1/(1-\delta))1/\eta_{ab}}{N_e N_p \Delta\Omega_e \Delta\Omega_p \frac{d\Omega^*}{d\Omega_p}\frac{\Delta\omega'}{\omega'}\omega'},$$

where

N_e ; number of electrons per monitor unit,
N_p ; number of target protons per square centimeter,
$\Delta\Omega_e$; solid angle of the electron detection system,
$\Delta\Omega_p$; solid angle of the proton detection system,
$\frac{d\Omega^*}{d\Omega_p}$; Jacobian factor,
$\frac{\Delta\omega'}{\omega'}$; momentum acceptance,
ω' ; momentum of the scattered electron,
Y ; true event yield per monitor unit,
η_e ; counting efficiency of the electron detection system,
η_p ; counting efficiency of the proton detection system,
δ ; radiative correction,
η_{ab} ; nuclear absorption correction.

These quantities have been mentioned in Chapter III and the previous sections of this Chapter.

In this experiment it was purposed to determine the form factors f_- and f_c at $q^2=3\mathrm{F}^{-2}$ by the procedure described in Chapter II. The measurement of the differential cross-section for the reaction $e+p\rightarrow e+N^*(1236)\rightarrow e+p+\pi^\circ$ were made in the region of the N^* (1236) responance for $\varepsilon=0.7$ and 0.5, respectively. Table 1 shows the kinematical conditions in these measurements. Because of the situation of the experimental area, two or more adjacent points of data were measured at a common setting angle, and as a result of it, the parameters q^2 and ε had slightly different values from the primarily intended ones of $q^2=3\mathrm{F}^{-2}$ and $\varepsilon=0.7$ and 0.5.

Table 1. The kinematical conditions for the cross-section measurements.

ω (MeV)	ω' (MeV)	θ (degree)	q^2 (F^{-2})	ε	M (MeV)
543	244	54.0	2.80	0.514	1154
609	250	54.0	3.22	0.487	1195
626	252	51.0	3.00	0.500	1211
681	259	48.0	3.00	0.500	1247
700	393	37.0	2.85	0.707	1160
755	406	37.0	3.17	0.692	1188
807	422	31.0	2.50	0.720	1227
881	440	31.0	2.84	0.702	1264
938	463	31.0	3.18	0.697	1284

Since the q^2- and ε-dependences of the cross-section are given from eq. (13) by

$$\frac{d^3\sigma(\theta^*=0)}{d\omega' d\Omega_e d\Omega^*}\propto\frac{1}{q^2}\,\frac{1}{1-\varepsilon}$$

except for the form factor term, the cross-section $d\sigma_1$ measured at ${q_1}^2$ and ε_1, which are slightly different from values ${q_0}^2$ and ε_0, was reduced to $d\sigma_0$ by multiplying a correction factor as follows:

$$d\sigma_0=d\sigma_1\frac{{q_1}^2}{{q_0}^2}\,\frac{1-\varepsilon_1}{1-\varepsilon_0}$$

Table 2. The measured values of the forward cross-section.

q^2 (F^{-2})	ε	M (MeV)	$\frac{d^3\sigma(\theta=0)}{d\omega' d\Omega_e d\Omega^*}$ ($cm^2/MeV\cdot sr^2$)
3.0	0.5	1154	$0.247\pm0.093\times10^{-35}$
		1195	0.749 ± 0.184
		1211	1.043 ± 0.228
		1247	0.799 ± 0.225
	0.7	1160	0.915 ± 0.234
		1188	1.821 ± 0.200
		1227	2.483 ± 0.278
		1264	1.632 ± 0.271
		1284	1.438 ± 0.370

The cross-section results thus obtained for $q^2=3F^{-2}$ and $\varepsilon=0.7$ and 0.5 are presented in Table 2. The correction mentioned above were less than 8 per cent except for one case of 23 per cent.

V. Results and Discussions

The cross-sections are plotted against the invariant mass M of the isobar for two values of the parameter ε, 0.5 and 0.7, as shown in Fig. 14. The dashed curves show the theoretical calculation following the Dalitz-Yennie formula[20], which is based on the Chew-Low static approximation. A detailed description of this calcultion was given by R. Kikuchi, et al.[21] The corresponding solid curves are those best-fitted to the experimental data by scaling down the ordinate of the theoretical curves. So far as the peak position and the width are concerned, the fitting of the resonance curve seems very good. In this fitting the highest-energy point of the observed data for $\varepsilon=0.7$ was

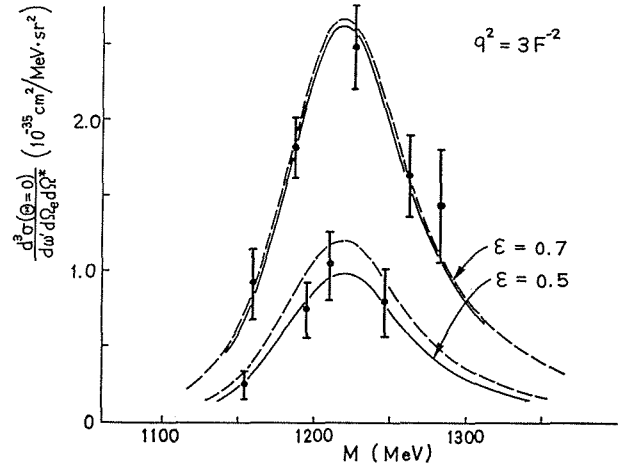

Fig. 14. The cross-section for the production of N^* (1236) by the reaction $e+p\rightarrow e+N^*$ from which the decay proton is emitted into the direction of N^*. The dashed curves show the theoretical cross-sections calculated by the Dalitz-Yennie formula and the solid curves are those best-fitted to the experimental data.

excluded, since the contribution of other reactions, such as the electroproduction of two pions could not be neglected at this energy.

Inasmuch as our present interest is to measure the cross-section for the reaction (1), it is necessary to subtract the contributions of non-resonant background from the observed cross-section. In the case of neutral pion photoproduction, however, almost all of the yield in the N^* (1236) region is considered to come from the resonant state, because there does not exist the peripheral process (which can not be neglected in the π^+ production), and the non-resonant Born term should be very small. It would be reasonably considered that the situation is the same also for the electroproduction.

Thus, by evaluating the area under the solid curves, we obtain the experimental values of the integrated cross-section for the electroproduction of N^* (1236) from which the decay proton is emitted to the forward direction:

$$\int \frac{d^3\sigma(\theta^*=0)}{d\omega' d\Omega_e d\Omega^*} dE = \begin{cases} 3.70 \pm 0.23 \text{ nb/sr}^2 & \text{for } \varepsilon = 0.7 \\ 1.38 \pm 0.18 \text{ nb/sr}^2 & \text{for } \varepsilon = 0.5. \end{cases} \tag{16}$$

From eq. (14), $f^2(q^2, \varepsilon)$ is obtained by substituting the observed cross-section (16) and the values of ω, ω' and M which correspond to the resonance peak (we regarded the location of the resonance peak as 1220 MeV for Fig. 14). The values of $f^2(q^2, \varepsilon)$ are

$$f^2(3\text{F}^{-2}, \varepsilon) = \begin{cases} 0.084 \pm 0.006 & \text{for } \varepsilon = 0.7 \\ 0.072 \pm 0.009 & \text{for } \varepsilon = 0.5 \end{cases} \tag{17}$$

and are plotted against ε in Fig. 15. Then fitting a straight line to these points, f_-^2 and $2q^2/|\boldsymbol{q}^*|^2 \cdot f_c^2$ are to be obtained as the intercept at $\varepsilon=0$ and the slope, respectively.

Although the inspection of Fig. 15 suggests apparently the existence of fairly large scalar contribution, we should note that there are the possible large uncertainties from the following reasons. Two points have the values of ε which are not much different from each other and far from the zero axis.

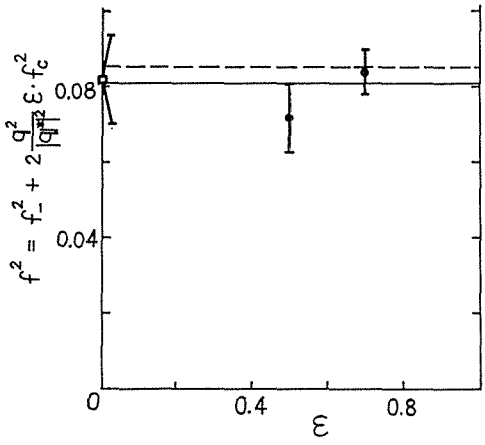

Fig. 15. The quantity $f_-^2(q^2) + (2q^2\varepsilon/|\boldsymbol{q}^*|^2) f_c(q^2)$ plotted against the polarization parameter ε. The Dalitz-Yennie prediction is represented by the dashed line. The experimental point on the $\varepsilon=0$ axis is taken from the π° photoproduction and non-coincidence electroproduction data (see text). The solid line represents the present results.

This situation might cause fairly iarge errors in evaluating the values of f_- and f_c.

On the other hand we can know the value of $(f_+^2+f_-^2)$ at $q^2=0$ to be 0.353 ± 0.001[22] from the analysis of the π° photoproduction data. Noting the well-known angular distribution $5-3\cos^2\theta^*$ for the π° photoproduction in the N^* (1236) region, we find the relation $f_+^2(0)=3f_-^2(0)$, which leads to $f_+^2(0)=0.259$ and $f_-^2(0)=0.086$. If we can assume that the q^2-dependence of $f_-^2(q^2)$ is not different from that of $f_+^2(q^2)+f_-^2(q^2)$ below $q^2=3\mathrm{F}^{-2}$, $f_-^2(3\mathrm{F}^{-2})$ is estimated from the transverse form factor data by the noncoincidence experiments of the electroproduction[3] to be 0.082 ± 0.012.

Allowing thus estimated value of $f_-^2(3\mathrm{F}^{-2})$ on the $\varepsilon=0$ axis in Fig. 15, it will be seen that the scalar contribution is likely to be negligibly small. If we assume that $f_c=0$, then the value of $f_-^2(3\mathrm{F}^{-2})$ is found to be 0.081 ± 0.005 from the $f^2(q^2, \varepsilon)$ data given by eq. (17).

The measurements of the γNN^* (1236) form factor were also reported by Ash et al.[4] and Mistretta et al.[6] Ash et al. defined the form factors $G_M^*(q^2)$, $G_E^*(q^2)$ and $G_C^*(q^2)$ corresponding to the M1, E2 and C2 multipole which contribute to the transition from $1/2^+$ to $3/2^+$. The relation between G^*'s they defined and f's are given by

$$\frac{G_M^{*2}+G_E^{*2}}{f_+^2+f_-^2}=\frac{G_C^{*2}}{f_0^2}=\frac{2M^2}{|\boldsymbol{q}|^2}=\frac{2m^2}{|\boldsymbol{q}^*|^2}. \tag{18}$$

If we asseme that only the magnetic dipole transition contributes to N^* (1236), as Ash et al. assumed $G_E^*=G_C^*=0$, it follows from eqs. (6.4) and (6.9) of ref. (8) that

$$f_+(q^2)=-\sqrt{3}f_-^2(q^2) \text{ and } f_c^2(q^2)=0. \tag{19}$$

Then using the above relations (18) and (19), the values of G_M^* of Ash et al.[4] at $q^2=3\mathrm{F}^{-2}$ and that of Mistretta et al.[6] at $q^2=3.3\mathrm{F}^{-2}$ correspond to $f_-^2(3\mathrm{F}^{-2})=0.089\pm0.013$, and $f_-^2(3.3\mathrm{F}^{-2})=0.111\pm0.010$, respectively.

As described before, the observed cross-section in the single arm experiments is integrated over the solid angle of the final hadron, hence the separation is made between $f_+^2+f^{-2}$ and f_c^2. In the coincidence measurement of the forward cross-section, on the other hand, the separation is made between f_-^2 and f_c^2. So, the form factors f_- and f_c can be determined separately by the Rosenbluth plot if the measurements are extended for wider range of ε in future experiments[23].

So far as N^* (1236) is concerned the contribution of the scalar photon seems to be negligibly small, however, it is expected that scalar excitation is more important for N^* (1525)[24], for instance. In the higher resonance region the radiative correction becomes critically important in the single arm experiment, while the situation is much advantageous for the coincidence experiment. Therefore the procedure of the Rosenbluth plot for the forward cross-section will be useful to investigate the excitation mechanism of the higher resonances.

ACKNOWLEDGEMENTS

The author wishes to express his sincere gratitude to Professors S. Yasumi, K. Miyake, Y. Kobayashi and S. Kaneko for their continuous encouragements

and guidances throughout this work. This experiment was performed by the colaboration of Professors Y. Kobayashi and S. Kaneko, Drs. K. Huke and R. Kikuchi, Messrs. T. Yamakawa and N. Kajiura, and the author. He is deeply indebted to Professors Y. Kobayashi and S. Kaneko for their generous leadership, and to Drs. K. Huke and R. Kikuchi for their valuable advices. The beam accomodation is mainly due to Mr. T. Yamakawa, and the computer system to Mr. N. Kajiura.

The author thanks the INS synchrotron crew and the Beam Extraction Group for their kind co-operations and hospitalities during the course of the experiment. His thanks are also due to Messrs. A. Okuda, M. Fujino, R. Hamatsu, T. Katsura, H. Kohno and T. Ohsugi for their generous assistance in carrying out the experiment.

He is sincerely grateful to Professor S. Hatano for his valuable discussions in preparing the manuscript. He also thanks Mrs. N. Endo for her typing of the manuscript.

REFERENCES AND FOOTNOTES

1) W. K. H. Panofsky and E. A. Allton, Phys. Rev. **110**, 1115 (1958).
2) L. N. Hand, Phys. Rev. **129**, 1834 (1963).
3) A. A. Cone, K. W. Chen, J. R. Dunning, Jr., G. Hartwig, N. F. Ramsey, J. K. Walker and R. Wilson, Phys. Rev. **156**, 1490 (1967); H. N. Lynch, J. V. Allaby and D. M. Ritson, ibid. **164**, 1635 (1967); W. Bartel, B. Dudelzak, H. Krehbiel, J. McElroy, U. Meyer-Berkhout, W. Schmidt, V. Walther and G. Weber, Phys. Letters **28B**, 148 (1968); F. W. Brasse, J. Engler, E. Ganssauge and M. Schweizer, Nuovo Cimento **45A**, 679 (1968); C. Betourne, C. Feautrier, J. Perez-y-Jorba and D. Treille, Nucl. Phys. **B5**, 355 (1968).
4) W. W. Ash, K. Berkelman, C. A. Lichtenstein, A. Ramanauskas and R. H. Siemann, Phys. Letters **24B**, 165 (1967).
5) C. W. Akerlof, W. W. Ash, K. Berkelman, C. A. Lichtenstein, A. Ramanauskas and R. H. Siemann, Phys. Rev. **163**, 1482 (1967).
6) C. Mistretta, J. A. Appel, R. J. Budnitz, L. Carrol, J. Chen, J. R. Dunning, Jr., M. Goitein, K. Hanson, D. C. Imrie and Richard Wilson, Phys. Rev. **184**, 1487 (1969).
7) K. Baba, N. Kajiura, S. Kaneko, K. Huke, R. Kikuchi, Y. Kobayashi and T. Yamakawa, Nuovo Cimento **59A**, 53 (1969).
8) J. D. Bjorken and J. D. Walecka, Ann. of Phys. 38, 35 (1966).
9) N. Christ and T. D. Lee, Phys. Rev. **143**, 1310 (1966).
10) In ref. (9) Christ and Lee defined the form factors $F_\pm$ and F_s which are similar to $f_\pm$ and f_0 defined by Bjorken and Walecka. However, we use the latter for convenience. The relation between f's and F's is given by
$\frac{f_+^2}{F_+^2}=\frac{f_-^2}{F_-^2}=\frac{2f_0^2}{F_s^2}=\frac{2mE}{M^2}$ and $\frac{f_e^2}{F_s^2}=\frac{|q^*|^2}{q_0^2}\cdot\frac{mE}{M^2}$.
11) This expression has been corrected as compared with eq. (6) in ref. (7). Integrating $\delta(E+\omega'-\omega-m)$ over E under constant q^2 and ε gives rise to the additional factor m/E instead of unity.
12) K. Huke, Y. Kobayashi, T. Yamakawa, S. Yamaguchi and S. Yamashita, Japanese Journ. Appl. Phys. 7, 1274 (1968).
13) E. A. Whalin, Jr. and R. A. Reitz, R. S. I. 26, 59 (1955).
14) S. Kabe, private communication.
15) N. Kajiura, SJC-T-67-1 (Report of Working Group for Construction of Proton Synchrotron, INS, Tokyo).
16) E. A. Allton, Phys. Rev. **135**, B570 (1964).
17) R. Hamatsu, Master Thesis, Hiroshima University (1968, unpublished).

18) J. D. Bjorken, Ann. of Phys. 24, 201 (1964).
19) N. Meister and D. R. Yennie, Phys. Rev. **130**, 1210 (1963).
20) R. H. Dalitz and D. R. Yennie, Phys. Rev. **105**, 1598 (1957).
21) R. Kikuchi, K. Baba, S. Kaneko, K. Huke, Y. Kobayashi and T. Yamakawa, Nuovo Cimento **43A**, 1178 (1966).
22) G. Fischer, H. Fischer, H. Kämpgen, G. Knop, P. Schultz and H. Wessels, Thirteenth Intern. Conf. on High Energy Physics, Berkeley (1966). The value quoted in the text corresponds to the value $G_M^*(0)=3.00\pm0.01$ given by Ash et al. in ref. (4) from the analysis of Fischer et al.'s data.
23) An experiment extending and refining the present experiment has been performed by the Tokyo INS group including the author himself. The result has shown that the scalar contribution is negligibly small. This work has been reported in Intern. Symposium on Electron and Photon Interactions at High Energies, Daresbury (1969) by N. Kajiura, K. Baba, R. Hamatsu, N. Ishihara, S. Kaneko, T. Katsura, T. Ohsugi, S. Fukui, M. Hongoh, T. Ohsuka, K. Ueno, K. Huke, T. Katayama, Y. Kobayashi and T. Yamakawa.
24) J. D. Walecka, Phys. Rev. **162**, 1462 (1967); P. L. Pritchett and P. A. Zucker, Phys. Rev. **D 1**, 175 (1970).